CHAPTER III

MIMO CAPACITY ANALYSIS WITH SPATIAL FADING CORRELATIONS

In this chapter, we will begin with model configuration of spatial fading correlations for mobile wireless communications. The MIMO system model and its problem definition in the channel capacity are raised when evaluating the integral form for cases of spatial correlation at the receiver side and spatial uncorrelated channel. The evaluation of integral form is proposed in the next section. Simulation condition, numerical results, and discussion will be carried out in the last sections.

3.1 Model Configuration of Spatial Correlations

3.1.1 Radio Wave Propagation of Mobile Wireless Communications

In this dissertation, it is important to understand and predict the correlation distribution between waveforms impinging on each antenna element in a variety of mobile and wireless environment. The property of fading correlation as function of antenna spacing in multi-element antenna system was first introduced in [89]. Figure 3.1 depicts the scatterer model used for examining the spatial fading correlation in a Non Line-of-Sight (NLoS) environment. A typical macrocellular radio - wave propagation environment is presented in Figure 3.1a, in which the Base Station (BS) is lifted in the cell, which means the BS is far away from a large number of local scatterers surrounding the Mobile Station (MS). For notation convenience, the MS and BS play the roles of transmitter and receiver, respectively. In other words, we consider an uplink communication system. It is reasonable to assume that there are linear arrays of antennas at the BS side and MS side, where the elements are spaced by d_{BS} and d_{MS}, respectively. The transmitter at the MS is normally assumed to be in

a discrete and uniform distribution surrounded by a cluster of many local scatterers in a circle, which implies that the signals impinging on the receiver at the BS arrive from all directions after bouncing from the surrounding scatterers. On the other hand, the receive antenna at the BS is unobstructed by the local scatterers due to the BS receive antenna located higher than and far away from the scatterers (Figure b). This is appropriate to be "single-ring" model initiated by Jackes [90]. The parameters in this model (Figure c) include the distance d from MS transmitter to BS receiver, the radius r of the ring of scatterers, the Angle-of-Departure (AoD) at the MS and Angle-of-Arrival (AoA) at the BS are θ and Ω, respectively, and the geometrical arrangement of the antenna sets. At the BS, the beamwidth of the incoming multi-paths are confined within 2Δ, where Δ is the angle spread. This angle is small and related with d and r through $\Delta \approx \arcsin(r/d)$. Furthermore, it is assumed that both d and r are usually large compared to the antenna spacings d_{BS} and d_{MS}. Generally, the following assumptions are made in the model [90]

i. Each effective scatterer $S(\theta)$ that lies at an angle θ to the MS is represented by a corresponding effective scatterer located at the same angle on the scatter ring centered on the MS. Effective scatterers are therefore assumed to be distributed uniformly in θ.

ii. Radio signals that are only reflected by the effective scatterers exactly once are considered. Moreover, all waves reaching the receive antennas are equal in power.

iii. The AoD probability density function (pdf) is assumed uniform. All users are assumed statistically independent with the same statistics.

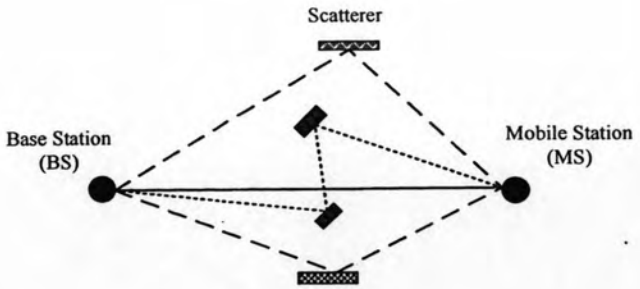

a) A typically macrocellular radio-wave propagation environment: directed signal (solid line), single-bounce (dashed line), and multiple-bounce (dotted line)

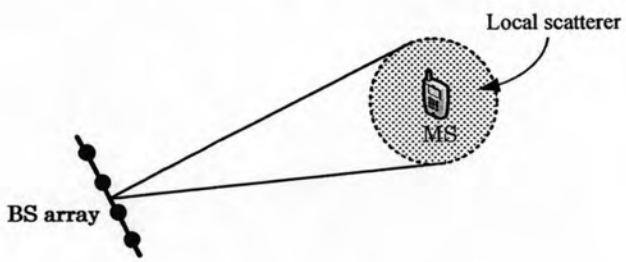

b) Local scatterer

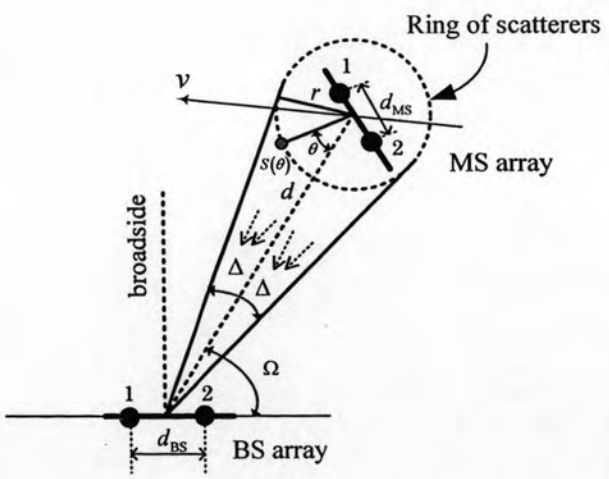

c) "single-ring" propagation model

Figure 3.1 Scattering model for examination of spatial fading correlation between the transmit antenna and the receive antenna

3.1.2 Spatial Correlation Characteristics

Many different scatterer distributions have been proposed in the literature, such as the uniform, Gaussian pdfs. In this dissertation, the von Mises angular pdf [91] is considered, which approximates many of these distributions and provides mathematical convenience leading to closed-form solutions for many problems. In [91], the authors showed that the von Mises pdf provided a good fit to measured results and was defined as

$$p^{scat}(\theta)=\frac{1}{2\pi I_0(k)}\exp\left[k\cos\left(\theta-\theta_p\right)\right];$$
$$\theta\in[-\pi,\pi), \tag{3.1}$$

where

- $I_0(\cdot)$ is the zero order modified Bessel function,
- $\theta_p\in[-\pi,\pi)$ is the mean direction of AoD at which the scatterers are distributed on the ring,
- $k\geq 0$ controls the width of AoD of scatterer components.

In Figure 3.2, the uniform distribution is illustrated for isotropic scattering: $p^{scat}(\theta)=1/2\pi$ for $k=0$ and $\theta_p=0$. When k increases, the scatterers become more clustered around θ_p and the scattering becomes increasingly nonisotropic.

When Δ is small, the scattering model often considers the case of fixed wireless communications. And the uniform angular distribution pdf (in Eq. (3.1)) is used with $k=0$ over $[0,2\pi]$ for the MS correlation. Based on the "single-ring" model in [90], the entries of correlation matrices for Rayleigh fading channel at the BS and MS antennas are respectively given by the following expressions:

$$\rho_{BS(1,2)} \approx J_0\left(2\pi \frac{d_{BS}}{\lambda}\left(\frac{r}{d}\right)\sin\Omega\right)^2 \times J_0\left(\frac{\pi d_{BS}}{\lambda}\left(\frac{r}{d}\right)^2 \sqrt{1-\frac{3}{4}\cos^2\Omega}\right)^2, \tag{3.2}$$

and

$$\rho_{MS(1,2)} \approx J_0\left(2\pi \frac{d_{MS}}{\lambda}\right), \tag{3.3}$$

where

- $J_0(x) = \frac{1}{2\pi}\int_0^{2\pi} \exp(jx\cos\theta)\,d\theta$ is the Bessel function of the first kind of the zero order.

The relationship between the absolute numerical values of the spatial correlation coefficients at the BS and the MS are illustrated in Figure 3.3 and Figure 3.4, respectively. At the BS antenna side, an example is if $d = 1000(m)$, $r = 6(m)$, then $\Delta \approx 0.006$. It can be found from results that the correlation coefficient decreases with an increase in the angular spread and the BS antenna separation (see Figure 3.3). The increased angular spread also implies that scatterers around the MS are more widely spaced, thereby increasing the distribution of time of arrival or excess delay.

At the MS antenna side, it can be observed that the minimum spacing between two antennas is about 0.4 wavelengths to achieve a zero correlation (see Figure 3.4). However, because the AoD's pdf is reduced below $[0, 2\pi]$, antenna spacing must be increased slightly to obtain small correlation. Practically, we can design an antenna configuration composed of several elements such as spatial, angular spread and polarization diversity to reduce the spacing for a required correlation.

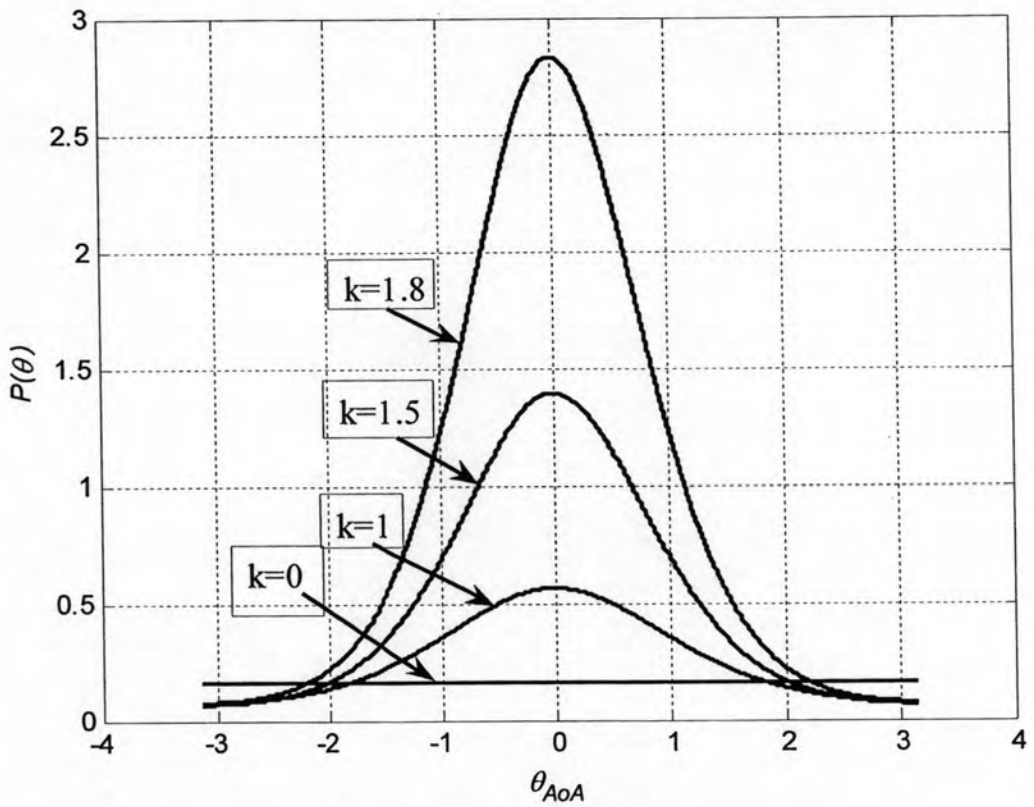

Figure 3.2 Multiple Von Misses distributions of scatterer components at the MS ($\theta_p = 0$). When *k=0,* the distribution is uniform and the scattering model is isotropic

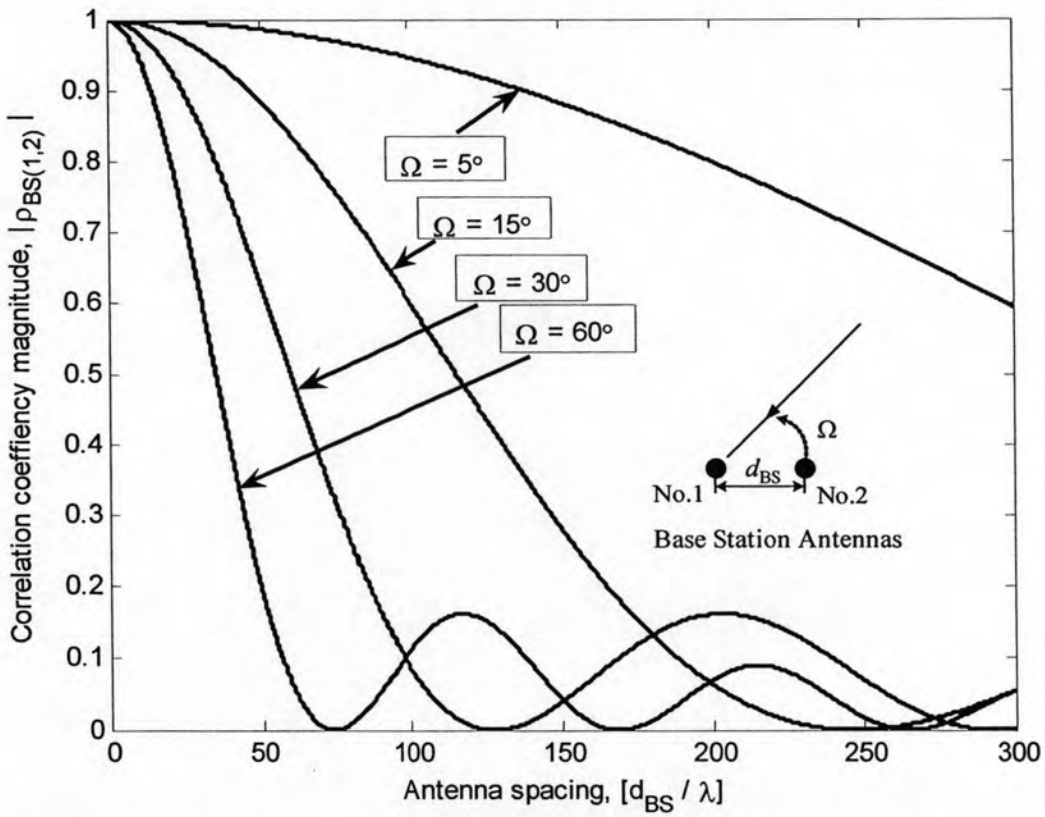

Figure 3.3 Spatial correlation characteristic at the BS antennas: magnitude of correlation coefficient versus antenna spacing for different angle Ω with the angle of incoming $\Delta \approx r / d = 0.006°$

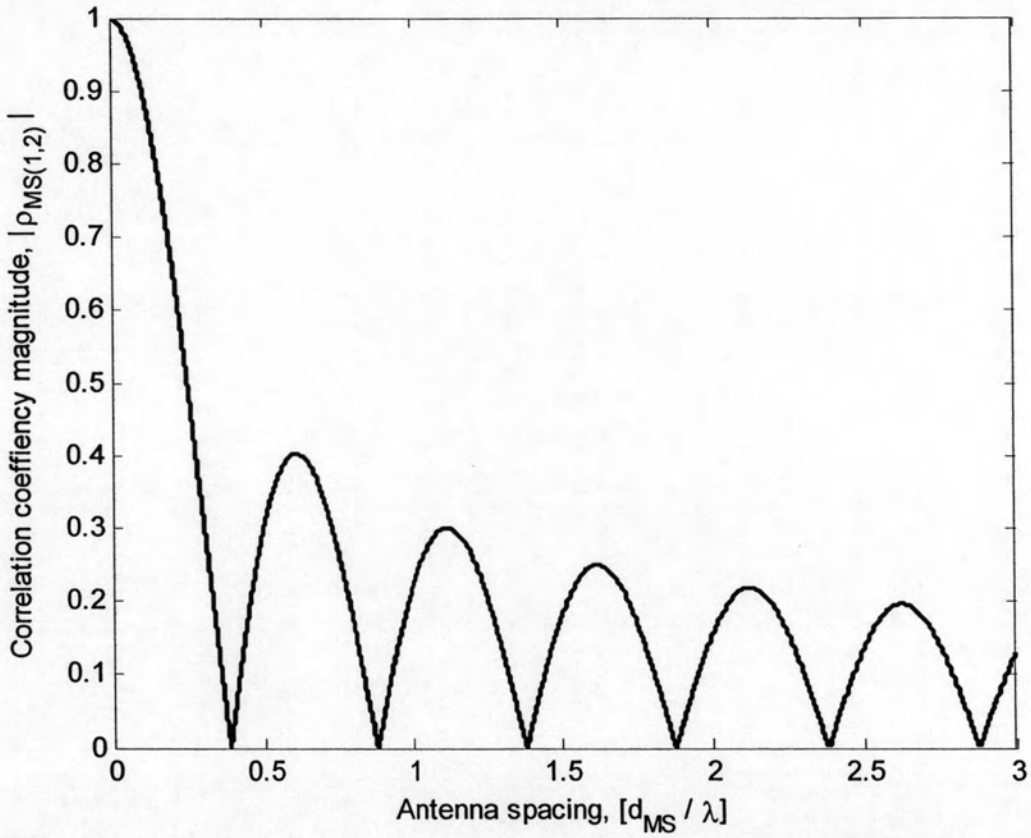

Figure 3.4 Spatial correlation characteristic at the MS antennas: magnitude of correlation coefficient versus antenna spacing

3.2 System Model

In this dissertation, considering a single-user and point-to-point narrowband Gaussian channel with N_T transmitter and N_R receiver antenna elements and refer to a $(N_T \times N_R)$ MIMO channel which subject to semi-correlated Rayleigh fading with spatial correlation at one side with the fewest number of antennas [74]. Mathematically, the complex baseband representation of the input-output relationship during a channel use $\mathbf{H}$ can be modeled as

$$\mathrm{y} = \mathbf{H}\mathrm{x} + \mathrm{n} \tag{3.4}$$

where

- $\mathrm{y} \in \mathbb{C}^{N_R}$ is the received signal vector,
- $\mathrm{x} \in \mathbb{C}^{N_T}$ is the input vector,
- x, y assumed to follow a Complex Circularly Symmetric Gaussian (CCSG) distribution subject to the average power constraint $E[\mathrm{x}^H \mathrm{x}] = P$,
- $\mathrm{n} \in \mathbb{C}^{N_R}$ is the zero-mean CCSG white noise vector, uncorrelated with x and with covariance $E[\mathrm{n}\mathrm{n}^H] = \sigma_n^2 \mathbf{I}_{N_R}$.

The channel matrix $\mathbf{H} \in \mathbb{C}^{N_R \times N_T}$ is zero-mean CCSG entries and is normalized such that $E[\mathrm{tr}(\mathbf{H}\mathbf{H}^\dagger)] = N_R N_T$. Under the separable correlation model [15], it is possible to express the channel matrix as

$$\mathbf{H} = \mathbf{\Psi}_R^{1/2} \mathbf{H}_W \mathbf{\Psi}_T^{1/2} \tag{3.5}$$

where

- $\mathbf{H}_{\mathrm{W}}$ is a white random matrix with zero-mean, unit variance CCSG entries, as denotes by $\mathbf{H}_{\mathrm{W}} \sim \widetilde{N}(0, \mathbf{I}_{N_{\mathrm{R}}} \otimes \mathbf{I}_{N_{\mathrm{T}}})$.
- $\mathbf{\Psi}_{\mathrm{T}} \in \mathbb{C}^{N_{\mathrm{T}} \times N_{\mathrm{T}}}$ and $\mathbf{\Psi}_{\mathrm{R}} \in \mathbb{C}^{N_{\mathrm{R}} \times N_{\mathrm{R}}}$ are denoted the covariance matrices of the columns and rows of $\mathbf{H}$ which represent the channel spatial correlation at the transmitter and receiver sides, respectively.

If $\mathbf{\Psi}_{\mathrm{T}} = \mathbf{I}_{N_{\mathrm{T}}}$ (or $\sigma^2 \mathbf{I}_{N_{\mathrm{T}}}$), and $\mathbf{\Psi}_{\mathrm{R}} = \mathbf{I}_{N_{\mathrm{R}}}$ (or $\sigma^2 \mathbf{I}_{N_{\mathrm{R}}}$), then the channel is called as spatial uncorrelated channel with Rayleigh distribution, and Eq. (3.5) becomes $\mathbf{H} = \mathbf{H}_{\mathrm{W}}$. This is a case of reasonable model for outdoor rich scattering areas in where multiple antenna systems are well-spaced.

In what follows, it is assumed that the channel matrix is random and that the receiver has perfect channel knowledge and no channel knowledge at the transmitter, and each transmitter antenna emitting an average power P / N_{T}. It is also assumed that the channel is memoryless, i.e., for each use of the channel an independent realization of $\mathbf{H}$ is drawn. This means that the capacity can be computed by the maximum of the mutual information over all input distributions. The results are also valid when $\mathbf{H}$ is generated by an ergodic process because as long as the receiver observes the $\mathbf{H}$ process, only the first statistics are needed to determine the channel capacity [16] by

$$E[C] = E\left[\log_2 \left| \mathbf{I}_n + \eta \mathbf{S} \right| \right], \tag{3.6}$$

where

- $\eta = P/(\sigma_n^2 N_{\mathrm{T}})$ is the normalized average SNR per receiver antenna under the power normalization,
- $\mathbf{S} \in \mathbb{C}^{N_{\mathrm{R}} \times N_{\mathrm{R}}} > 0$ is the random Wishart matrix and is defined by

$$\mathbf{S} \triangleq \begin{cases} \mathbf{H}\mathbf{H}^H, & \text{if } N_{\mathrm{T}} \geq N_{\mathrm{R}} \\ \mathbf{H}^H\mathbf{H}, & \text{otherwise.} \end{cases} \tag{3.7}$$

The expectation $E[\cdot]$ is evaluated using a complex singular Wishart density. Be noted that in general condition, the $N_R \times N_T$ MIMO channel $(N_T \geq N_R)$ can be represented by the N_R orthogonal subchannels with gaining $\{\lambda_1 \geq \lambda_2 \geq \ldots \geq \lambda_{N_R}\}$ which are eigenvalues of **S**. Therefore, the average (or mean) capacity (in Eq. (3.6)) can be rewritten as

$$E[C] = \sum_{i=1}^{N_R} E\left[\log_2(1+\eta\lambda_i)\right], \tag{3.8}$$

Let $P(\mathbf{\Lambda})$ denotes the distribution of the eigenvalues of **S** where $\mathbf{\Lambda} = diag(\lambda_1, \lambda_1, \ldots, \lambda_{N_R})$ is arranged in descending order. The channel ergodic capacity can now be evaluated by integrating over the distribution $P(\mathbf{\Lambda})$ by

$$E[C] = \underbrace{\int_0^\infty \cdots \int_0^\infty}_{N_R\text{-fold}} \sum_{i=1}^{N_R} \log_2(1+\eta\lambda_i) P(\mathbf{\Lambda}) d\mathbf{\Lambda}. \tag{3.9}$$

We now motivate to find the pdf of the eigenvalues of the complex Wishart matrix. By integrating over the distribution of the eigenvalues of **S** as opposed to the distribution of **H**, the order of integration is reduced from $2N_T N_R$ to N_R.

3.2.1 Spatial correlation at the receiver side

In this subsection, the distribution of the eigenvalues of **S** is presented for the case of the spatial correlation at the receiver. This analysis can be easily modified for a study of the spatial correlation at the transmitter by interchanging the subscripts T and R.

From Eq. (2.15) from chapter 2, if $L = \mathbf{I}_{N_T}, \mathbf{\Psi}_T = \mathbf{I}_{N_T}$, then the distribution of the ordered joint eigenvalues of the complex Wishart matrix as distributed as complex Wishart with N_T mean and $\mathbf{\Psi}_R$ variance: $\mathbf{S} \sim \widetilde{W}_{N_R}(N_T, \mathbf{\Psi}_R)$. As a result, the case of the spatial correlation at the receiver side is raised. By scaling this distribution by the

factor of $1/N_{\mathrm{R}}!$, the distribution of the unordered eigenvalues of a complex Wishart matrix is given by

$$P^{semi}(\mathbf{\Lambda}) = \frac{\pi^{N_{\mathrm{R}}(N_{\mathrm{R}}-1)}}{N_{\mathrm{R}}!\left|\mathbf{\Psi}_{\mathrm{R}}\right|^{N_{\mathrm{R}}}\tilde{\Gamma}_{N_{\mathrm{R}}}(N_{\mathrm{R}})\tilde{\Gamma}_{N_{\mathrm{R}}}(N_{\mathrm{T}})} \times \prod_{i<j}^{N_{\mathrm{R}}}\left(\lambda_i-\lambda_j\right)^2\prod_{j=1}^{n}\lambda_j^{N_{\mathrm{T}}-N_{\mathrm{R}}} \times {}_0\widetilde{F}_0^{(N_{\mathrm{R}})}\left(-\mathbf{\Psi}_{\mathrm{R}}^{-1},\mathbf{\Lambda}\right). \tag{3.9}$$

The channel ergodic capacity would be uncomplicated to evaluate on condition that Eq. (3.9) does not include the hypergeometric function of two matrix arguments ${}_0\widetilde{F}_0^{(N_{\mathrm{R}})}\left(-\mathbf{\Psi}_{\mathrm{R}}^{-1},\mathbf{\Lambda}\right)$, which is generally expressed as a series expansion on zonal polynomials. However, this formulation is not easy for numerical work, as zonal polynomials are well known for being extremely difficult to calculate and the series expansion is slow to converge. Fortunately, a more tractable formulation has been proposed in [92], where the hypergeometric function of two matrix arguments can be derived from the terms of classical hypergeometric functions as

$${}_0\widetilde{F}_0^{(n)}(S,T) = \frac{\left|{}_0F_0\left(s_it_j\right)\right|}{V(S)V(T)} \times \prod_{j=1}^{n}(j-1)!;$$

with

$$\begin{cases} {}_0F_0\left(s_it_j\right) \triangleq \begin{bmatrix} {}_0F_0\left(s_1t_1\right) & \cdots & {}_0F_0\left(s_1t_n\right) \\ \vdots & \ddots & \vdots \\ {}_0F_0\left(s_nt_1\right) & \cdots & {}_0F_0\left(s_nt_n\right) \end{bmatrix}, \\ V(S) \triangleq \prod_{i<j}^{n}\left(s_i-s_j\right), \\ V(T) \triangleq \prod_{i<j}^{n}\left(t_i-t_j\right), \end{cases} \tag{3.10}$$

where

- S, T are $(n \times n)$ Hermitian matrices with real eigenvalues $s_1,\ldots,s_n$ and $t_1,\ldots,t_n$, respectively.
- ${}_0F_0(x) = \exp(x)$ is the classical hypergeometric function.

The formulations in (3.10) also require that the eigenvalues of the matrices S and T are unequal. Therefore, ${}_0\widetilde{F}_0^{(N_R)}\left(-\boldsymbol{\Psi}_R^{-1}, \boldsymbol{\Lambda}\right)$ can now be rewritten by

$$ {}_0\widetilde{F}_0^{(N_R)}\left(-\boldsymbol{\Psi}_R^{-1}, \boldsymbol{\Lambda}\right) = \frac{\left|\exp\left(\lambda_i \psi_j\right)\right|}{\prod_{i<j}^{N_R}\left(\lambda_i - \lambda_j\right)\left(\psi_j - \psi_i\right)} \times \prod_{k}^{N_R}(k-1)!, \tag{3.11} $$

where

- $\psi_1,\ldots,\psi_{N_R}$ are the eigenvalues of $\boldsymbol{\Psi}_R^{-1}$, arranged in descending order.

Substituting Eq. (3.11) into Eq. (3.9) yielding the distribution of the unordered eigenvalues of S can now be calculated by

$$ P^{semi}(\boldsymbol{\Lambda}) = \frac{\pi^{N_R(N_R-1)}\left|\boldsymbol{\Psi}_R\right|^{-N_R}\left|\exp\left(\lambda_i \psi_j\right)\right|}{N_R!\,\tilde{\Gamma}_{N_R}(N_R)\tilde{\Gamma}_{N_R}(N_T)} \times \frac{\prod_{i<j}^{N_R}\left(\lambda_i - \lambda_j\right)\prod_{i<j}^{N_R}\lambda_i^{N_T - N_R}\prod_{k=1}^{N_R}(k-1)!}{\prod_{i<j}^{N_R}\left(\psi_j - \psi_i\right)}. \tag{3.12} $$

3.2.2 Spatial uncorrelated channel

In this subsection, the distribution of the eigenvalues of $\mathbf{S}$ is presented where spatial uncorrelated channel at both the transmitter and the receiver sides is accounted. In this case, if $L = \mathbf{I}_{N_T}, \boldsymbol{\Psi}_T = \mathbf{I}_{N_T}$ and $\boldsymbol{\Psi}_R = \sigma^2 \mathbf{I}_{N_R}$, then from Eq. (2.15),

the unordered joint eigenvalue density of the complex Wishart matrix $\mathbf{S} = \mathbf{H}\mathbf{H}^H \sim \widetilde{W}_{N_R}(N_T, \sigma^2 \mathbf{I}_{N_R})$ is given by

$$P^{un}(\mathbf{\Lambda}) = \frac{\pi^{N_R(N_R-1)}\left(\sigma^2\right)^{-N_T N_R}}{N_R!\,\tilde{\Gamma}_{N_R}(N_R)\tilde{\Gamma}_{N_R}(N_T)} \exp\left(-\frac{1}{\sigma^2}\sum_{i=1}^{N_R}\lambda_i\right) \times \prod_{i<j}^{N_R}\left(\lambda_i-\lambda_j\right)^2 \prod_{j=1}^{N_R}\lambda_j^{N_T-N_R}. \tag{3.13}$$

The channel ergodic capacities are obtained by substituting (3.12) and (3.13) into (3.9) and evaluating the integral numerically.

3.3 The Proposed Closed-Form Evaluation of Integral Form

By carefully examining Equations (3.9), (3.12), and (3.13), it is easily seen that evaluating channel capacity leads to evaluating the integral form of the following type

$$\Xi(\beta,\eta,\lambda) \triangleq \int_0^\infty x^\beta \times \log_2(1+\eta x) \times \exp(-\lambda x)\,\mathrm{d}x; \quad \eta,\lambda > 0, k \in \mathbb{N}^*, \tag{3.14}$$

To the best of our knowledge, this type of integral cannot be solved analytically in closed-form expression using standard tables of integrals or standard integration techniques and classical reference books, such as in [88]. For this reason, we pursue an approach in close-form for evaluating this integral, in term of Meijer's *G*-functions.

By using [93], Eq. (11), the integral in Eq. (3.14) can be expressed in closed-form expression by using the algorithmic and exponential functions in terms of Meijer's *G*-functions as

$$\log_2(1+\eta x) = \log_2(e) \times G_{2,2}^{1,2}\left[\eta x \,\middle|\, \begin{matrix} 1, & 1 \\ 1, & 0 \end{matrix}\right], \tag{3.15}$$

and

$$\exp(-\lambda x) = G_{0,1}^{1,0}\left[\lambda x \left| \begin{matrix} - \\ 0 \end{matrix} \right. \right], \tag{3.16}$$

respectively, in which $G[\cdot]$ is the Meijer's G-function and is defined in the Appendix A. These functions are of very natural and contain basically all known elementary functions as special cases, which are included as functions built-in most of the standard mathematical software packages such as Maple or Mathematica. Numerical evaluation of these functions is immediately feasible.

Substituting Eq. (3.15) and Eq. (3.16) into Eq. (3.14), then the integral form therefore can be expressed as

$$\Xi(\beta,\eta,\lambda) = \log_2(e) \int_0^\infty x^\beta \, G_{2,2}^{1,2}\left[\eta x \left| \begin{matrix} 1,1 \\ 1,0 \end{matrix} \right. \right] G_{0,1}^{1,0}\left[\lambda x \left| \begin{matrix} - \\ 0 \end{matrix} \right. \right] dx, \tag{3.17}$$

Again, by using [93], Eq. (21), then the above integral can be expressed in closed-form expression as

$$\begin{aligned} \Xi(\beta,\eta,\lambda) &= \frac{\sqrt{k}\,\log_2(e)}{\eta^{(\beta+1)}\left(\sqrt{2\pi}\right)^{(k+2l-3)}} \\ &\times G_{2l,\,k+2l}^{k+2l,\,l}\left[\left(\frac{\lambda}{k}\right)^k \frac{1}{\eta^l} \left| \begin{matrix} \Delta(l,-(\beta+1)),\,\Delta(l,-\beta) \\ \Delta(k,0),\,\Delta(l,-(\beta+1)),\,\Delta(l,-(\beta+1)) \end{matrix} \right. \right], \end{aligned} \tag{3.18}$$

where

- $\Delta(n,\xi) \triangleq \xi/n,(\xi+1)/n,\ldots,(\xi+n-1)/n,$

- ξ is an arbitrary real value, and n is a positive integer. Whereas k and l are positive integers and chosen for satisfying $l/k=1$.

In the particular case of $k=l=1$, Eq. (3.18) becomes

$$\Xi(\beta,\eta,\lambda)=\frac{\log_2(e)}{\eta^{\beta}}\,G_{2,3}^{3,1}\left[\frac{\lambda}{\eta}\middle|\begin{matrix}(-\beta),\,(-\beta+1)\\(-\beta),\,(-\beta),\,0\end{matrix}\right], \tag{3.19}$$

Furthermore, [94], Eq. (8.2.2.15), pp. 521 expresses a relationship

$$z^k\,G_{p,q}^{m,n}\left[z\middle|\begin{matrix}(a_p)\\(b_q)\end{matrix}\right]=G_{p,q}^{m,n}\left[z\middle|\begin{matrix}k+(a_p)\\k+(b_q)\end{matrix}\right], \tag{3.20}$$

where

- $(a_p)=a_1,a_2,\ldots,a_p$;
- $(b_p)=b_1,b_2,\ldots,b_q$

Therefore, the integral form in Eq. (3.20) can be simply evaluated in the following form

$$\Xi(\beta,\eta,\lambda)=\frac{\log_2(e)}{\lambda^{\beta}}\,G_{2,3}^{3,1}\left[\frac{\lambda}{\eta}\middle|\begin{matrix}0,\,1\\0,\,0,\,\beta\end{matrix}\right]. \tag{3.21}$$

This type of integral form is a less simple expression and is different from the derived method provided in [95] Appendix B, in which the integral form is given in a form of the complementary incomplete Gamma function.

3.4 Monte Carlo Method

Numerical methods which involve sampling from random number are called Monte-Carlo Method [96]. It can also be loosely described as statistical simulation

methods, where statistical simulation is defined in quite general terms to be any method that utilizes sequences of random number to perform the simulation. In fact, Monte-Carlo methods have been used for centuries, but only in the past several decades it has the technique gained the status of a full-fledged numerical method capable of addressing the most complex applications. The only requirement is that the physical (or mathematical) system can be described by pdf's, which can be met in most occasions. The simulations are performed (multiple 'trials' or 'histories') based on the samples which are generated from the pdf and in this way some mathematics characteristics can be obtained. From the law of large numbers, it is shown that the outcome estimation is non-biased estimation when the number of sample is big enough [97].

3.5 Simulation Condition

For a more in-depth analysis of the performance of MIMO systems, simulations are conduct to investigate the effects of SNR and spatial correlation on MIMO channel capacity. First, a simulation model is presented. Then simulation will be done to observe how antenna correlation and SNR would affect the average channel capacity in the various scenarios of uncorrelated and semi-correlated fading channel. The simulation conditions and parameters are summarized Table 3.1.

In the analysis, the narrowband channel response is modeled by a non-zero mean complex Gaussian process. In the correlated channel, we will simulate a correlated channel matrix using a correlated-based channel model as follows,

$$\mathbf{H} = \mathbf{\Psi}_{\mathrm{R}}^{1/2}\mathbf{H}_{\mathrm{W}}\mathbf{\Psi}_{\mathrm{T}}^{1/2} \tag{3.22}$$

where

- $\mathbf{H}_{\mathrm{W}} \in \mathbb{C}^{N_{\mathrm{R}} \times N_{\mathrm{T}}}$ contains iid (uncorrelated) complex Gaussian entries with zero mean and unit variance,
- $\mathbf{\Psi}_{\mathrm{R}}$ and $\mathbf{\Psi}_{\mathrm{T}}$ are the normalized correlation matrices at the receiver and transmitter, respectively.

Table 3.1 Simulation Condition

Parameter	Value
Number of Tx antennas (N_T)	2, 4, 6, 8, 10
Number of Rx antennas (N_R)	2
Antennas pattern	Omni-directional in Azimuth
Fading type	Flat Rayleigh channel
Path-loss model	Free-space model
Carrier frequency	5.2 [GHz]
Power allocation	Equal at Tx antennas
Spatial correlation	At Rx side
Synchronization	Perfect
Channel realizations	100000
Simulation method	Monte Carlo simulation

The correlation coefficient at the receiver side (and the transmitter as well) ranges from 0 to 1 and models the correlation between two neighboring receive (transmitter) antennas. With the given channel model, correlation between two antenna elements decreases exponentially with their distance.

The potential gain of the MIMO concept strongly depends on the correlation coefficient between the elements of $\mathbf{H}$. Base on the "single ring" model, the entries of the correlation matrices for the Rayleigh fading channel at the BS and the MS between two elements are given in [72] by $\rho_{BS(1,2)}$, $\rho_{MS(1,2)}$, respectively.

Given $\rho_{BS(1,2)}$ and $\rho_{MS(1,2)}$, the MIMO system investigated here uses various numbers of antennas at the BS and only two antennas at the MS. The spatial correlation at the transmitter is temporarily ignored, and with correlation only at the MS side. Therefore, the transmitter spatial correlation matrix $\mathbf{\Psi}_T$ is set to the identity matrix and the Rx symmetrical correlation matrix of $\mathbf{\Psi}_R$ is as follows

$$\Psi_T = \begin{bmatrix} 1 & \rho_{MS(1,2)} \\ \rho_{MS(1,2)} & 1 \end{bmatrix} \tag{3.23}$$

In the simulations, the SNR is varied and Monte Caro simulations are conduct to obtain the average channel capacity. At a given SNR, the number of antennas at the transmitter is varied whereas the number of antenna at the receiver is fixed to 2. Under the fixed transmit power P, the MIMO channel capacities corresponding to each channel respond can be analyzed. Then, the average channel capacity with respect to the average received SNR for the various values of correlation coefficient will be estimated by averaging over 100000 realizations of $\mathbf{H}$, and over all possible antenna pairs, j to i. we assume that the average receiver SNR, as defined in Section 2, should be high enough for low-error-rate communication. If SNR is too low, we need very complex codes improve enough redundancy to combat the noise so that we can recover the desired signal with low error probability at the receiver.

Finally, the SNR in dB is defined by

$$\gamma_{dB} = 10 \cdot \log_{10}\left(\frac{P}{\sigma_n^2}\right) = 10 \cdot \log_{10}(\gamma) \quad [\text{dB}]. \tag{3.24}$$

3.6 Simulation Results and Discussion

Hereafter, in order to corroborate the analysis conducted in previous sections, we present numerical evaluation of ergodic capacities for various channel matrices with / without spatial correlation at the MS and compared to simulation results. We also suppose that there is no spatial correlation at the BS and the number of the MS antennas is restricted to 2.

In the first numerical example, we consider an $(N_T \times 2)$ MIMO system with various numbers of antennas at the BS and only two antennas at the MS, and with correlation only at the MS side. A typical example of this scenario is for uplink communication from the MS to the BS, where the antennas at the BS can be spaced sufficiently far enough in rich scattering environments to achieve spatial uncorrelated results among them at the receiver side. On the other hand, practically, it is not easy

and not constructive to space the antennas far apart at the mobile unit due to constraints of physical size. As a result, the spatial correlation arises among the antenna elements in such scenario, i.e., $\mathbf{S} \sim \widetilde{W}_2(N_T, \mathbf{\Psi}_R)$ is a complex Wishart matrix. The unordered joint eigenvalue density is given by (in Eq. (3.12))

$$P^{semi}(\lambda_1,\lambda_2) = \frac{(\psi_1\psi_2)^{N_T}(\lambda_1\lambda_2)^{N_T-2}(\lambda_1-\lambda_2)}{2(\psi_2-\psi_1)\Gamma(N_T)\Gamma(N_T-1)} \times\left[\exp(-\psi_1\lambda_1-\psi_2\lambda_2)-\exp(-\psi_1\lambda_2-\psi_2\lambda_1)\right]. \tag{3.25}$$

The MIMO system investigated here uses the spatial correlation coefficient described in Section 2, except that the spatial correlation at the transmitter is temporarily ignored. Therefore, $\mathbf{\Psi}_T$ is set to the identity matrix and the elements of $\mathbf{\Psi}_R$ are set to $\rho_{MS(1,2)} = 0.9$ (in Eq. (3.25)). The receiving covariance matrix is given as

$$\mathbf{\Psi}_R = \begin{bmatrix} 1 & 0.9 \\ 0.9 & 1 \end{bmatrix}, \tag{3.25}$$

in which the eigenvalues are 1.9 and 0.1. Hence $\psi_1 = 1/1.9$ and $\psi_2 = 1/0.5$ are the eigenvalues of $\mathbf{\Psi}_R^{-1}$. Figure 3.5, Figure 3.6, Figure 3.7, Figure 3.8, Figure 3.9, and Figure 3.10 illustrate the pdfs of the eigenvalues $P^{semi}(\lambda_1,\lambda_2)$ (in Eq. (3.25)) for 2×2, and 4×2 MIMO Rayleigh channels, and various correlation coefficients (i.e. 0.3, 0.5, and 0.9), where the two peaks are firstly small and spread out afterwards.

In Figure 3.11, the solid lines represent the analytical results with the help of (3.21). These lines are compared to the circles, which represent Monte Carlo simulation results. Each simulation point averages over 10^6 random Rayleigh channel realizations with specific SNR and number of the transmitting and receiving antennas. The results are for the ergodic capacity with various antenna configurations $(N_T = 2, N_R = 2)$, $(N_T = 4, N_R = 2)$, $(N_T = 8, N_R = 2)$, and $(N_T = 10, N_R = 2)$. From the Figure 6, it can be seen that the ergodic capacity significantly increases as is higher

SNR and as the number of transmitting antennas increases, and the curves obtained by Eq. (3.9), Eq. (3.12) and Eq. (3.21) match well with Monte-Carlo simulations.

Second, we consider the scenario with spatial uncorrelated Rayleigh $(N_T \times 2)$ channels among the antenna elements at both the BS and the MS sides. A situation arises when the antenna elements at both the MS transmitter and the BS receiver are spaced sufficiently far apart from each other i.e., the unordered joint eigenvalues density of $\mathbf{S} \sim \widetilde{W}_2(N_T, \mathbf{I}_2)$ is given by (in Eq. (3.13))

$$P^{un}(\lambda_1, \lambda_2) = \frac{(\lambda_1 \lambda_2)^{N_T-2}(\lambda_1 - \lambda_2)^2}{2\Gamma(N_T)\,\Gamma(N_T-1)} \times \left[\exp(-\lambda_1 - \lambda_2)\right]. \tag{3.26}$$

Figure 3.12 shows the ergodic capacity of MIMO systems for the uncorrelated Rayleigh (iid) channels, versus the SNR with varying antenna configurations. Again, the solid lines representing the analytical results are compared to the circles representing Monte Carlo simulation results. As expected, the ergodic capacity is improved with an increase in the number of antennas and SNR's. The good agreement between the analytical and simulation results verifies the accuracy of our analysis formulas.

Figure 3.13 compares numerical results for semi-correlated and uncorrelated Rayleigh channels with correlation coefficient $\rho_{MS(1,2)} = 0.9$. It can be observed that although the capacity performance of correlated MIMO Rayleigh $(N_T \times 2)$ channels is degraded compared to the uncorrelation in such channels, MIMO systems can be sufficiently efficient and more robust than antenna correlation when increasing the number of the transmitting antennas and increasing SNR.

A different behavior can be observed in Figure 3.14 for different MIMO channels $(N_T = 2, 4, 6, 8, 10$ and fixed $N_R = 2)$ for SNR = 20dB. For correlation coefficients greater than approximately 0.9 at the receiver side, there is a significant degradation in channel ergodic capacity.

From these discussions, we summarize chapter the followings

i) the ergodic (average) capacity is significantly increased with an increase in the number of antennas at the BS and SNR.

ii) in the presence of high spatial fading correlation at the MS, the channel capacity scales linearly with respect to N_T and degrades compared with the case of iid Rayleigh channel.

iii) the correlation coefficients are greater than approximately 0.9 at the MS, there is a significant degradation in channel ergodic capacity.

Table 3.2 depicts the channel capacity in bits/s/Hz for (Nt x 2) uncorrelated Rayleigh fading channel matrix, note that each column represents different levels of input power or signal-to noise ratio (SNR) in dB. Table 3.3 shows the capacity for (Nt x 2) semi-correlated Rayleigh fading channel matrix with correlation coefficient of 0.9.

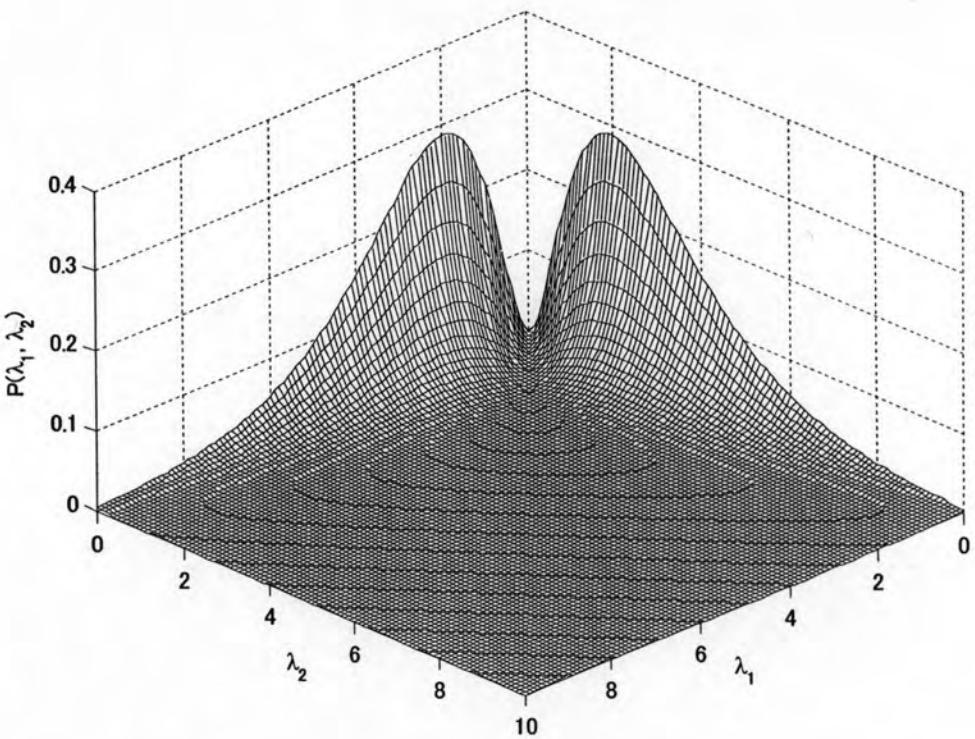

Figure 3.5 Distribution of the eigenvalues $P(\lambda_1, \lambda_2)$ of correlated Wishart matrix $\mathbf{S} = \mathbf{H}\mathbf{H}^H$ for a 2×2 MIMO Rayleigh channel with $\rho_{\mathrm{MS}(1,2)} = 0.3$

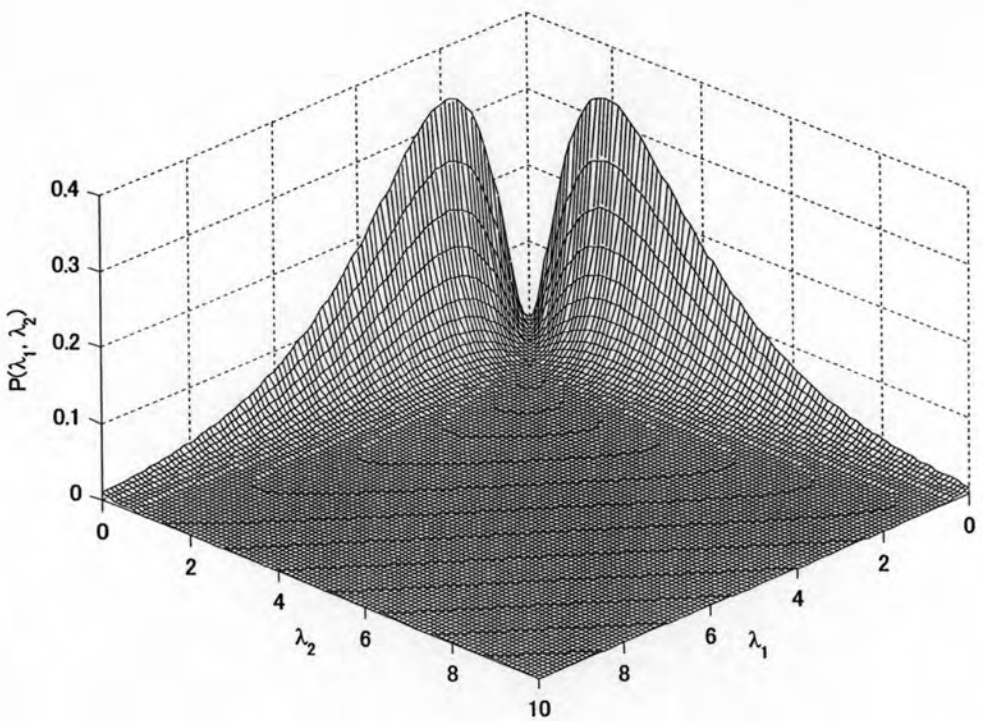

Figure 3.6 Distribution of the eigenvalues $P^{semi}(\lambda_1, \lambda_2)$ of correlated Wishart matrix $\mathbf{S} = \mathbf{H}\mathbf{H}^H$ for a 2×2 MIMO Rayleigh channel with $\rho_{\mathrm{MS}(1,2)} = 0.5$

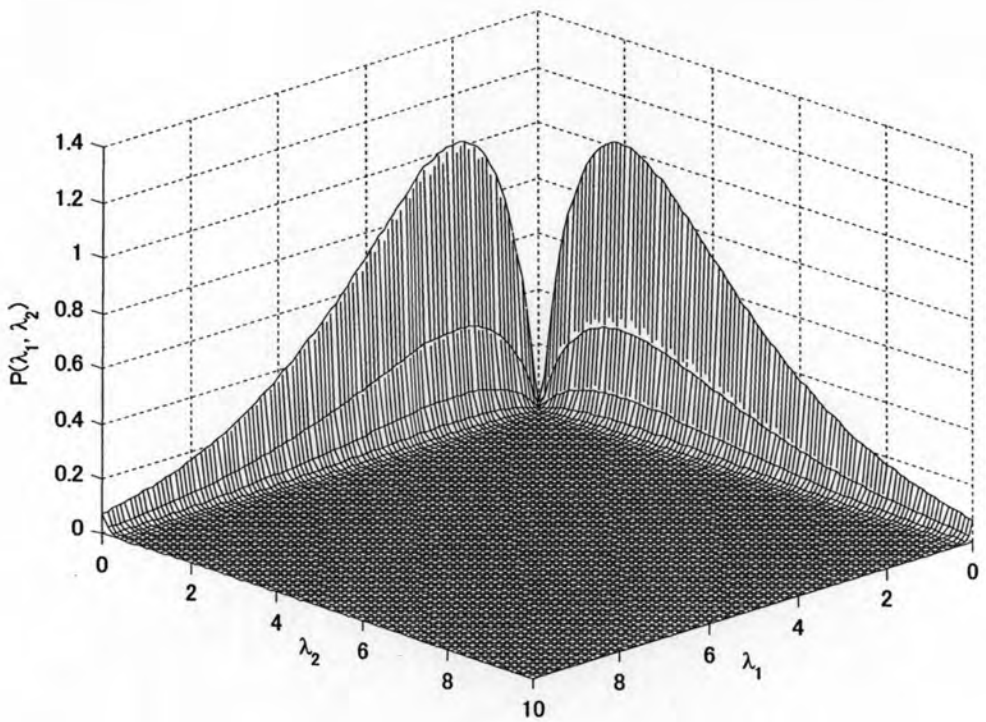

Figure 3.7 Distribution of the eigenvalues $P^{semi}(\lambda_1, \lambda_2)$ of correlated Wishart matrix $\mathbf{S} = \mathbf{H}\mathbf{H}^H$ for a 2×2 MIMO Rayleigh channel with $\rho_{\mathrm{MS}(1,2)} = 0.9$

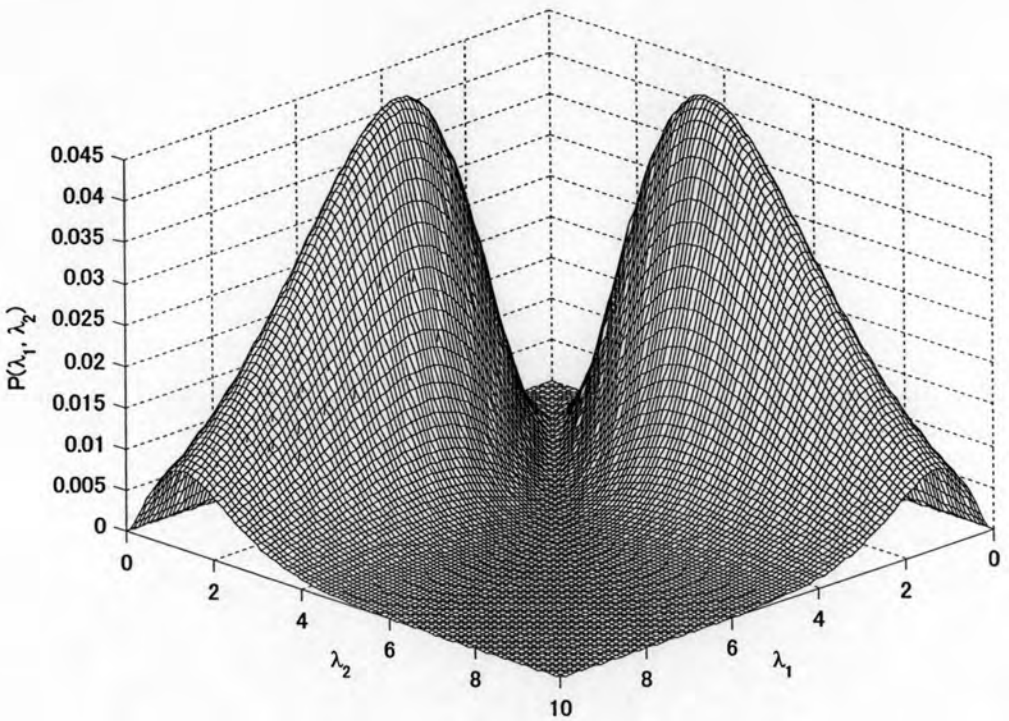

Figure 3.8 Distribution of the eigenvalues $P^{semi}(\lambda_1, \lambda_2)$ of correlated Wishart matrix $\mathbf{S} = \mathbf{H}\mathbf{H}^H$ for a 4×2 MIMO Rayleigh channel with $\rho_{\mathrm{MS}(1,2)} = 0.3$

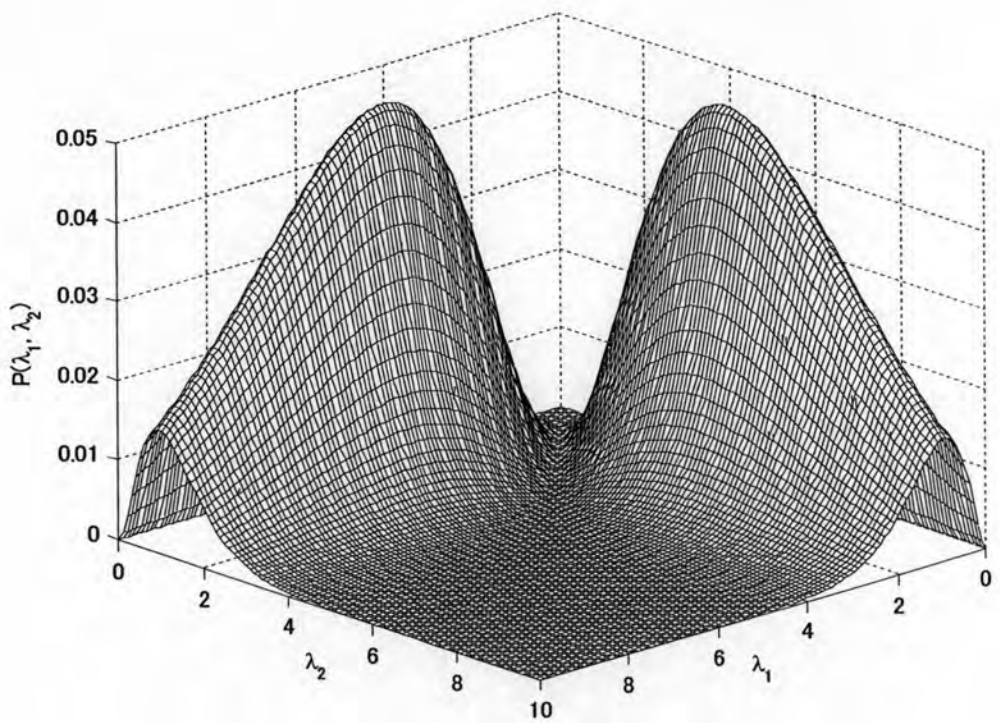

Figure 3.9 Distribution of the eigenvalues $P^{semi}(\lambda_1, \lambda_2)$ of correlated Wishart matrix $\mathbf{S} = \mathbf{H}\mathbf{H}^H$ for a 4×2 MIMO Rayleigh channel with $\rho_{\mathrm{MS}(1,2)} = 0.5$

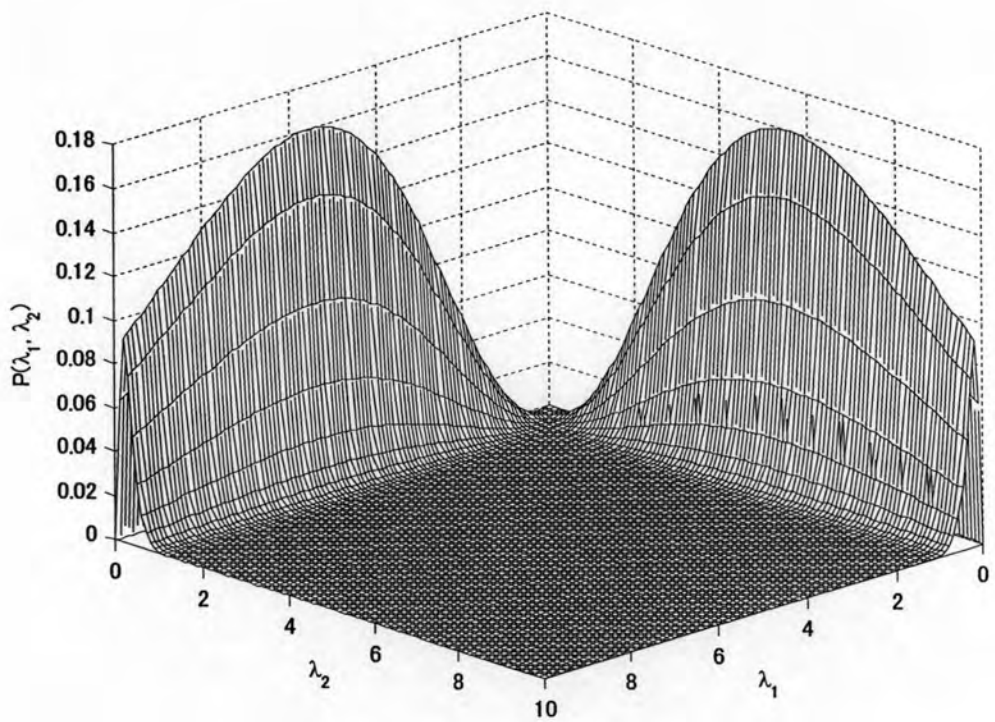

Figure 3.10 Distribution of the eigenvalues $P^{semi}(\lambda_1, \lambda_2)$ of correlated Wishart matrix $\mathbf{S} = \mathbf{H}\mathbf{H}^H$ for a 4×2 MIMO Rayleigh channel with $\rho_{\mathrm{MS}(1,2)} = 0.9$

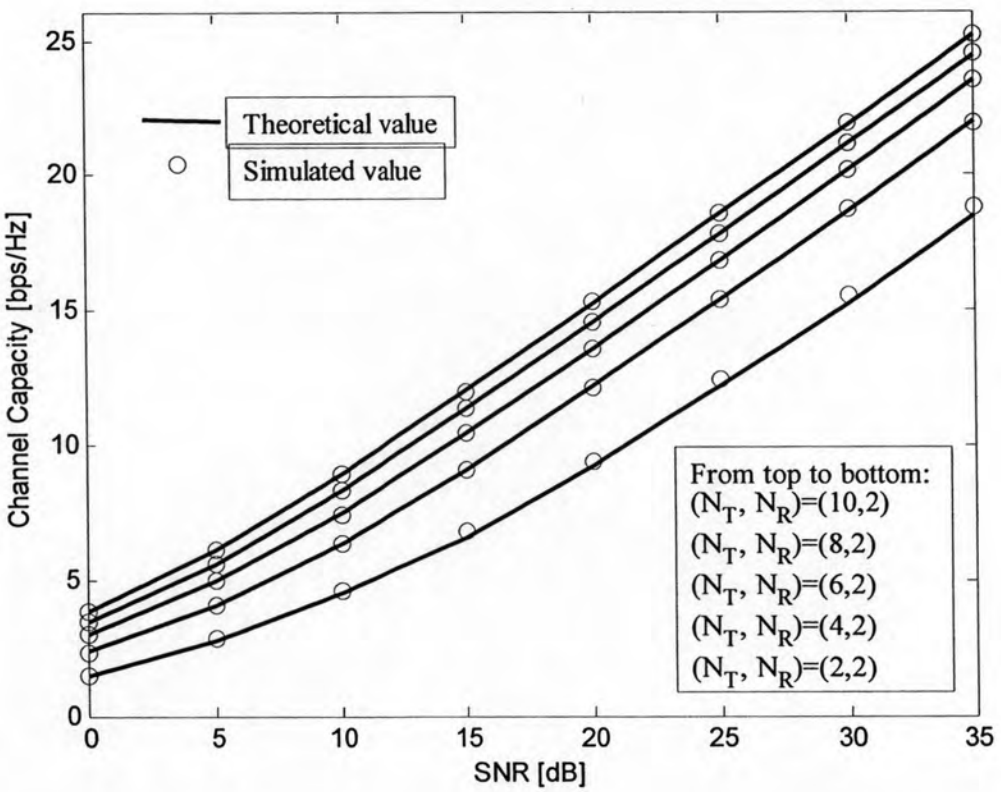

Figure 3.11 Capacity of semi-correlated MIMO Rayleigh channel at the MS under comparison of theoretical and simulated results with $\rho_{MS(1,2)} = 0.9$

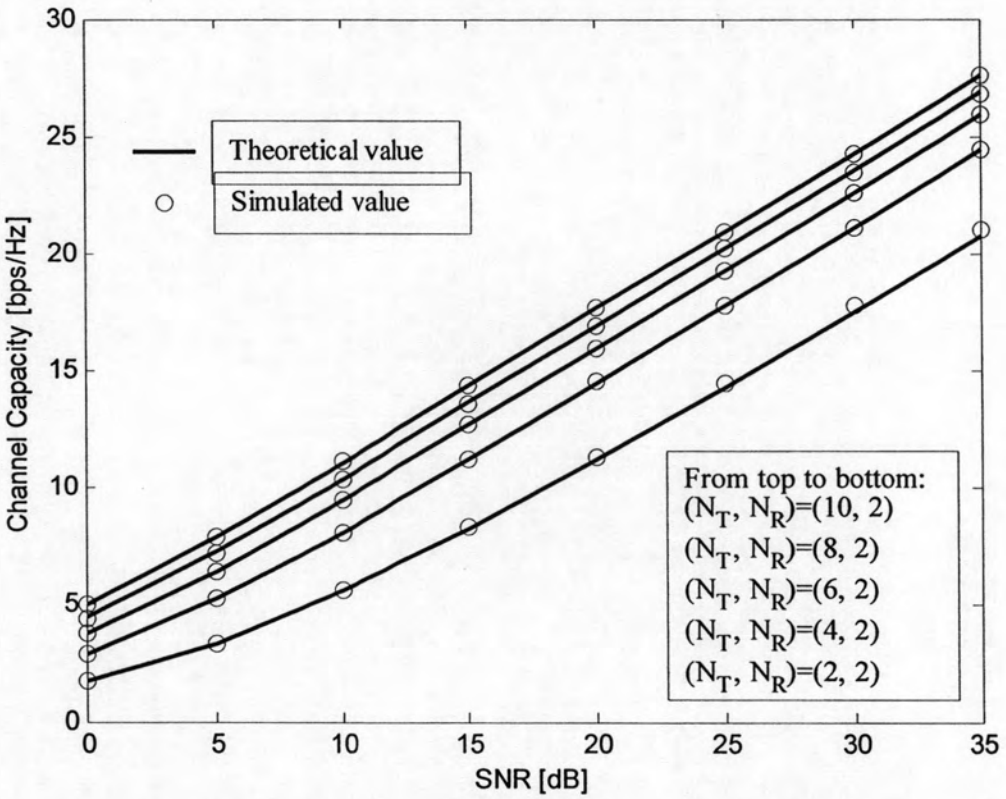

Figure 3.12 Capacity of uncorrelated MIMO Rayleigh channel under the comparison of theoretical and simulated results

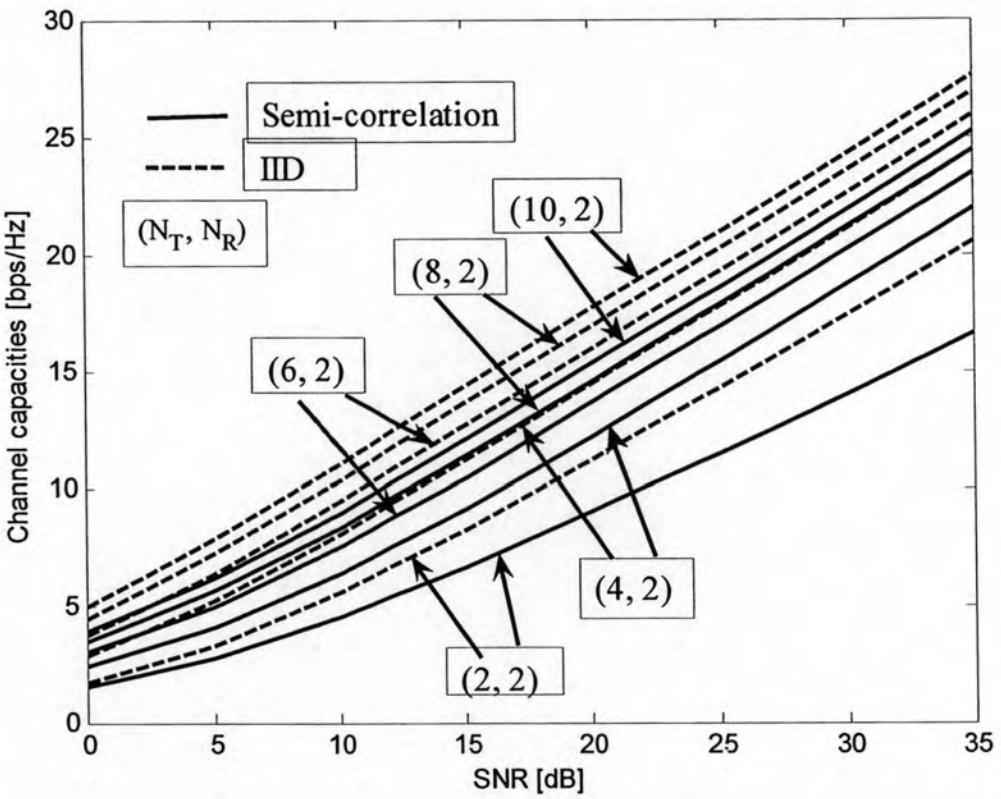

Figure 3.13 Comparison of the numerical results in capacity of semi-correlated and uncorrelated MIMO Rayleigh channels with $\rho_{MS(1,2)} = 0.9$

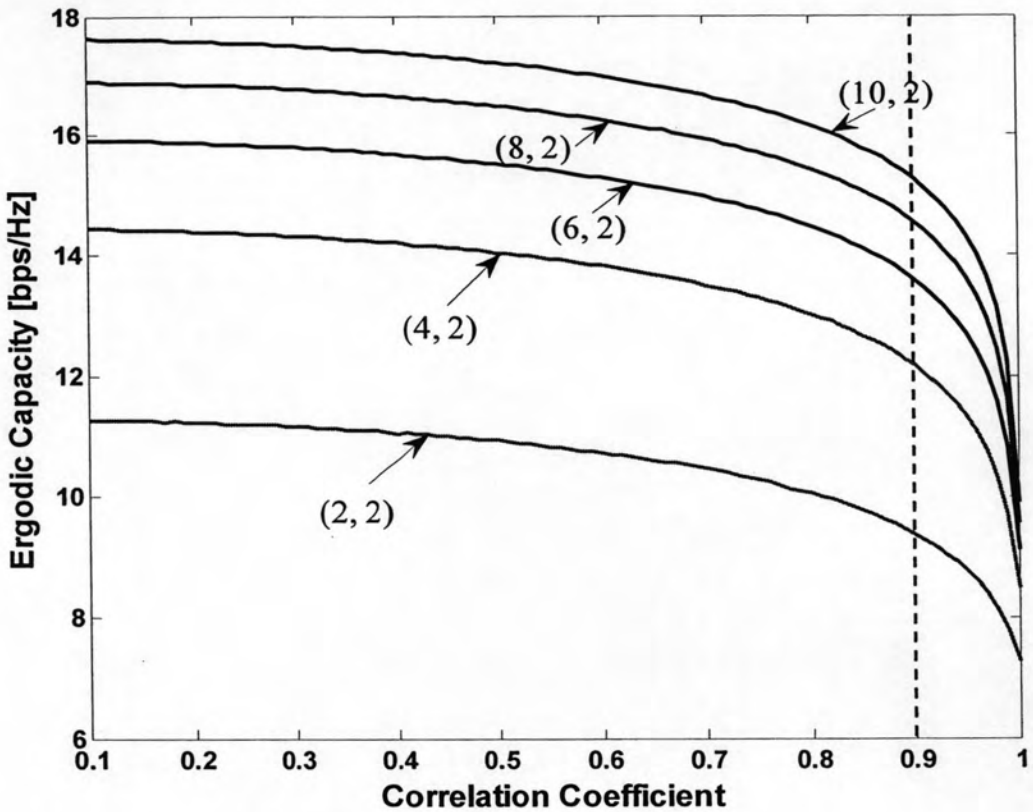

Figure 3.14 Capacity as a function of correlation coefficient for SNR=20dB and different MIMO channels, with fixed $N_R = 2$, varying $N_T = 2, 4, 6, 8, 10$

Table 3.2 MIMO Rayleigh uncorrelated (iid) channel: comparison of numerical / simulated results

Nt	SNR in dB							
	0 dB	5 dB	10 dB	15 dB	20 dB	25 dB	30 dB	35 dB
2	1.6838/1.6809	3.3023/3.2990	5.5374/5.5389	8.23290/8.2554	11.2001/11.2773	14.2917/14.4650	17.4300/17.7312	20.5839/21.0312
4	2.8610/2.8731	5.1807/5.1967	8.04850/8.0662	11.1974/11.2153	14.4597/14.4778	17.7623/17.7803	21.0781/21.0960	24.3981/24.4159
6	3.7304/3.7295	6.3659/6.3656	9.41710/9.4172	12.6451/12.6454	15.9364/15.9367	19.2485/19.2488	22.5674/22.5676	25.8884/25.8885
8	4.4108/4.4093	7.2164/7.2144	10.3478/10.3456	13.6058/13.6036	16.9071/16.9049	20.2226/20.2202	23.5424/23.5401	26.8637/26.8614
10	4.9665/4.9680	7.8764/7.8785	11.0518/11.0542	14.3254/14.3279	17.6318/17.6344	20.9489/20.9514	24.2692/24.2718	27.5908/27.5932

Table 3.3 MIMO Rayleigh semi-correlated (at the receiver) channel: comparison of numerical / simulated results

Nt	SNR in dB							
	0 dB	5 dB	10 dB	15 dB	20 dB	25 dB	30 dB	35 dB
2	1.4946/1.4848	2.7775/2.8012	4.495/4.5519	6.5846/6.7536	8.9481/9.3673	12.205/12.2958	15.2712/15.4258	18.5148/18.6849
4	2.3960/2.3636	4.1010/4.0948	6.3649/6.3508	9.11120/9.1135	12.1820/12.1589	15.4085/15.4017	18.6941/18.7116	21.9997/22.0096
6	2.9842/2.9825	4.9626/4.9663	7.4807/7.4812	10.4235/10.4208	13.5998/13.6089	16.8721/16.8636	20.1780/20.176	23.4951/23.4979
8	3.4672/3.4706	5.6146/5.6208	8.2889/8.2899	11.3310/11.3248	14.5514/14.5492	17.8394/17.8321	21.1506/21.1432	24.4686/24.4705
10	3.867/3.8726	6.1413/6.1322	8.9214/8.9152	12.022/12.0218	15.2662/15.2745	18.5626/18.5648	21.8764/21.8789	25.1957/25.1861